

# Facile synthesis of pure non-monoclinic zirconia nanoparticles and their catalytic activity investigations for Knoevenagel condensation†

Cite this: *RSC Adv.*, 2013, **3**, 22353

Reihaneh Malakooti,<sup>\*a</sup> Hesamaldin Mahmoudi,<sup>a</sup> Rahele Hosseinabadi,<sup>a</sup> Srebri Petrov<sup>b</sup> and Andrea Migliori<sup>c</sup>

Zirconia nanoparticles were synthesized by the non-hydrolytic thermal decomposition of zirconyl chloride octahydrate in the presence of oleylamine and oleic acid. The nanoparticles were characterized by XRD, HR-TEM and EDAX techniques. TEM observation confirmed that the nanoparticles have an approximately spherical shape with an average size of 3–4 nm and a non-monoclinic structure. Unlike previous approaches, our synthesis of the catalytically relevant (tetragonal and/or cubic) phase of this material did not require (i) an annealing step to stabilize the tetragonal phase, or (ii) the inclusion of dopants. Furthermore, these high surface area tetragonal zirconia nanoparticles showed a good catalytic activity towards the Knoevenagel condensation.

Received 16th June 2013

Accepted 4th September 2013

DOI: 10.1039/c3ra44682d

[www.rsc.org/advances](http://www.rsc.org/advances)

## 1. Introduction

Research on zirconium dioxide ( $\text{ZrO}_2$ ) has attracted great interest because of its useful applications in ceramics,<sup>1</sup> wear-resistant optical coatings,<sup>2</sup> catalysts,<sup>3</sup> fuel cell electrolytes,<sup>4</sup> buffer layers for superconductor growth,<sup>5</sup> oxygen sensors,<sup>6</sup> and gate dielectrics.<sup>7</sup> Zirconia exhibits three common phases: monoclinic, tetragonal and cubic. At atmospheric pressures, the monoclinic phase is stable at room temperature and converts to the tetragonal phase at 1170 °C, and then to the cubic phase at 2370 °C. While the monoclinic phase is stable at standard temperature and pressure, the other two phases are known to be more catalytically active. Therefore, the stabilization of the non-monoclinic phases at room temperature has been the subject of several investigations.<sup>8</sup> Typically, stabilization is obtained (i) by doping with CaO,  $\text{Y}_2\text{O}_3$ , MgO or  $\text{CeO}_2$ ,<sup>9</sup> or (ii) by decreasing the size of the particle.<sup>10</sup> Garvie proposed that the tetragonal phase is stable below a critical size of about 10 nm, while the monoclinic phase is stable above approximately 30 nm.<sup>10b</sup> According to previous studies, the formation of the tetragonal phase is favoured at high surface-to-volume ratios (*i.e.*, small sizes) because of the relatively lower surface free energy than the

monoclinic structure.<sup>11</sup> Several methods have been used to synthesize undoped tetragonal  $\text{ZrO}_2$  nanoparticles.<sup>11c–15</sup>

They typically require (i) difficult procedures, (ii) careful control of reaction parameters such as temperature, pressure, and pH, (iii) the use of relatively expensive and toxic zirconium alkoxides, or (iv) annealing (an energy-intensive process which leads to the sintering and growth of nanoparticles, and likely reduces the catalyst activity and its surface area).

Here we report a simple one-step synthesis of  $3.7 \pm 1.1$  nm tetragonal  $\text{ZrO}_2$  nanoparticles, based on the thermal decomposition of zirconyl chloride octahydrate ( $\text{ZrOCl}_2 \cdot 8\text{H}_2\text{O}$ ) in the presence of oleic acid and oleylamine surfactants. The catalytic activity of the zirconia nanoparticles was tested against the Knoevenagel condensation, one of the most common and versatile reactions for C–C bond formation. The combination of structural characterization and catalytic activity studies suggested that the tetragonal  $\text{ZrO}_2$  nanoparticles with high surface area are highly active in the Knoevenagel reaction.

## 2. Experimental section

### 2.1 Materials

Oleylamine was obtained from Aldrich. Other materials were purchased from Merck. All materials were used without further purification.

### 2.2 Characterizations

X-ray diffraction (XRD) data were recorded with a Bruker D8 Advance with Ni-filtered  $\text{Cu K}\alpha$  radiation (1.5406 Å). Data were obtained with a speed of  $2^\circ \text{min}^{-1}$  and a step of  $0.05^\circ$ . Crystal parameters were calculated by Rietveld refinement. The  $\text{N}_2$

<sup>a</sup>Nanochemistry Research Laboratory, Department of Chemistry, University of Birjand, Birjand, Iran. E-mail: rmalakooti@birjand.ac.ir

<sup>b</sup>Lash Miller Chemical Laboratories, Department of Chemistry, University of Toronto, 80 St. George Street, Toronto, ON, M5S 3H6, Canada

<sup>c</sup>Consiglio Nazionale delle Ricerche, CNR-IMM, Area della Ricerca di Bologna, Via Gobetti 101, 40126 Bologna, Italy

† Electronic supplementary information (ESI) available. See DOI: 10.1039/c3ra44682d

sorption analysis was measured at 77 K using a [5.0.0.3] Belsorp, BEL Japan, Inc. instrument. Before measurements, the samples were outgassed at 100 °C for 4 h. Using the Brunauer–Emmett–Teller (BET) method and Barrett–Joyner–Halenda (BJH) analyses the specific surface area and the pore size distributions, respectively, were obtained from the desorption branch of the isotherms. Transmission electron microscopy (TEM) and High Resolution TEM (HR-TEM) were performed with a Philips Tecnai F20 operating at 200 kV. For this purpose, the crystal powders were dispersed in isopropyl alcohol using ultrasound and a few drops of the suspension were deposited on a sample holder consisting of a copper grid covered with holey carbon film. The chemical composition was determined on several crystal grains by means of energy dispersive spectrometry (EDS) by using an EDAX Phoenix spectrometer equipped with an ultra-thin window detector and TIA analysis software. <sup>1</sup>H-NMR spectra were recorded on a Bruker AC 400 spectrometer. Chemical shifts ( $\delta$ ) were expressed in parts per million (ppm) and were referenced to deuterated solvents with tetramethylsilane as the internal standard. Coupling constants were expressed in Hertz (Hz). Melting points (M.P.) were measured on an Electrothermal 9100 apparatus and were uncorrected. Mass spectra were recorded on a Shimadzu GCMS-QP5050 mass spectrometer operating at an ionization potential of 70 eV. IR spectra were measured on a Perkin-Elmer 783 infrared spectrophotometer.

### 2.3 Preparation of zirconia nanoparticles

In a typical synthesis, 3 mmol of  $\text{ZrOCl}_2 \cdot 8\text{H}_2\text{O}$ , 3 mmol of oleic acid and 8.4 mL of oleylamine were mixed in a 25 mL three-neck flask equipped with a magnetic stirrer, a condenser, and a thermocouple. The resulting mixture was degassed and dehydrated at 120 °C for 30 min under vacuum. This mixture was then heated to 300 °C under an  $\text{N}_2$  flow and aged at this temperature for 1 h. The turbid mixture was then cooled to room temperature by removing the heat source. The white precipitate was retrieved by centrifugation and dried after washing with methanol and toluene three times. In the case of the annealed samples, the white solid was calcined in a furnace at 400 °C or 600 °C for 2 h.

### 2.4 General procedure for the Knoevenagel condensation of aldehydes and malononitrile

In a typical condensation reaction,  $\text{ZrO}_2$  (0.02 g) was added to a stirred solution of the corresponding aldehyde (1 mmol) and malononitrile (1.2 mmol) in ethanol (5 mL). The reaction mixture was refluxed for specified times until thin layer chromatography (TLC) indicated the complete disappearance of the starting material (eluent, *n*-hexane–EtOAc, 5 : 1). The catalyst was isolated by filtration. The product was crystallized in ethanol and no further purification was required.

The structure of the products was confirmed by IR, <sup>1</sup>H-NMR and mass spectra and comparison with authentic samples prepared by previously reported methods.<sup>16–24</sup> Selected data for typical products are given below.

**2-Benzylidenemalononitrile (2a).** White crystals, (146 mg, 95%). M.P. = 84–85 °C. <sup>1</sup>H NMR ( $\text{CDCl}_3$ , 400 MHz)  $\delta$ : 7.93 (d,  $J$  = 7.8 Hz, 2H, Ar), 7.79 (s, 1H, =CH), 7.64 (d,  $J$  = 7.5 Hz, 1H, Ar), 7.55 (d,  $J$  = 7.2 Hz, 2H, Ar). IR (KBr)  $\nu$ : 2223 (CN), 1591 (C=C)  $\text{cm}^{-1}$ ; MS (70 eV)  $m/z$ : 154 ( $\text{M}^+$ ).

**2-(4-Methoxybenzylidene)malononitrile (2b).** Yellow crystals, (168 mg, 91%). M.P. = 112–114 °C, <sup>1</sup>H NMR ( $\text{CDCl}_3$ , 400 MHz)  $\delta$ : 7.91 (d,  $J$  = 8.8 Hz, 2H, Ar), 7.65 (s, 1H, =CH), 7.01 (d,  $J$  = 8.8 Hz, 2H, Ar), 3.92 (s, 3H, Me); IR (KBr)  $\nu$ : 2225 (CN), 1560 (C=C)  $\text{cm}^{-1}$ ; MS (70 eV)  $m/z$ : 184 ( $\text{M}^+$ ).

**2-(4-Methylbenzylidene)malononitrile (2c).** Pale yellow crystals, (153 mg, 91%). M.P. = 132–133 °C, <sup>1</sup>H NMR ( $\text{CDCl}_3$ , 400 MHz)  $\delta$ : 7.83 (d,  $J$  = 8.2 Hz, 2H, Ar), 7.64 (s, 1H, =CH), 7.50 (d,  $J$  = 9.8, 2H, Ar), 2.45 (s, 3H, Me); IR (KBr)  $\nu$ : 2228 (CN), 1584 (C=C)  $\text{cm}^{-1}$ ; MS (70 eV)  $m/z$ : 168 ( $\text{M}^+$ ).

**(2,4-Dimethylbenzylidene)malononitrile (2f).** Yellow crystals, (200 mg, 91%). M.P. = 143–145 °C, <sup>1</sup>H NMR ( $\text{CDCl}_3$ , 400 MHz)  $\delta$ : 8.26 (d,  $J$  = 8.8 Hz, 1H, Ar), 8.18 (s, <sup>1</sup>H, =CH), 6.61 (dd,  $J$  = 8 Hz,  $J$  = 2 Hz, <sup>1</sup>H, Ar), 3.93 (s, 3H, Me), 3.92 (s, 3H, Me); IR (KBr)  $\nu$ : 2220 (CN), 1600 (C=C)  $\text{cm}^{-1}$ ; MS (70 eV)  $m/z$ : 182 ( $\text{M}^+$ ).

**2-(3-Nitrobenzylidene)malononitrile (2h).** White crystals, (187 mg, 94%). M.P. = 101–102 °C, <sup>1</sup>H NMR ( $\text{CDCl}_3$ , 400 MHz)  $\delta$ : 8.66 (s, 1H), 8.49 (d,  $J$  = 7.0 Hz, 1H), 8.34 (d,  $J$  = 7.9, 1H), 7.88 (s, 1H), 7.82 (t,  $J$  = 7.7 Hz, 1H); IR (KBr)  $\nu$ : 2233 (CN), 1533 (C=C)  $\text{cm}^{-1}$ ; MS (70 eV)  $m/z$ : 199 ( $\text{M}^+$ ).

**2-(2-Chlorobenzylidene)malononitrile (2i).** White crystals, (177 mg, 94%). M.P. = 87–89 °C, <sup>1</sup>H NMR ( $\text{CDCl}_3$ , 400 MHz)  $\delta$ : 8.28 (s, 1H, =CH), 8.20 (d,  $J$  = 7.8 Hz, 1H, Ar), 7.55–7.59 (m, 3H, Ar); IR (KBr)  $\nu$ : 2232 (CN), 1590 (C=C)  $\text{cm}^{-1}$ ; MS (70 eV)  $m/z$ : 188 ( $\text{M}^+$ ).

## 3. Results and discussion

### 3.1 Characterization

Fig. 1 compares the XRD patterns of zirconia nanoparticles – before and after annealing at temperatures of 400 or 600 °C – with those of bulk zirconia. The XRD pattern obtained before annealing (Fig. 1a) displays broad peaks which complicate the identification of the crystal phase. Rietveld refinement was performed to identify the zirconia polymorph and a good fit was obtained for the tetragonal phase with lattice parameters  $a$  = 3.463 Å and  $c$  = 5.092 Å (ESI†). The decreased size of the unit cell compared with standard values<sup>25</sup> ( $a$  = 3.61 Å and  $c$  = 5.27 Å) is related to the partial reduction of  $\text{ZrO}_2$  and the formation of oxygen vacancies which play an important role in stabilizing the tetragonal structure in nanocrystalline zirconia.<sup>26</sup> The size of the crystalline grains obtained by Rietveld refinement was estimated to be below 2 nm. As shown in Fig. 1d, the bulk zirconia standard (purchased from Merck) only exhibits the monoclinic phase. Crystallites of these sizes are more correctly characterized as clusters. Their atomic structure should be compared to those of bulk samples with caution, coming from the knowledge that substantial structural differences can exist (in both the bulk and the surface structure).<sup>27</sup> The XRD patterns obtained from the annealed samples (*cf.* Fig. 1b and c) indicate a mixture of phases in various ratios. The phase content was estimated from XRD data by the Rietveld method and the

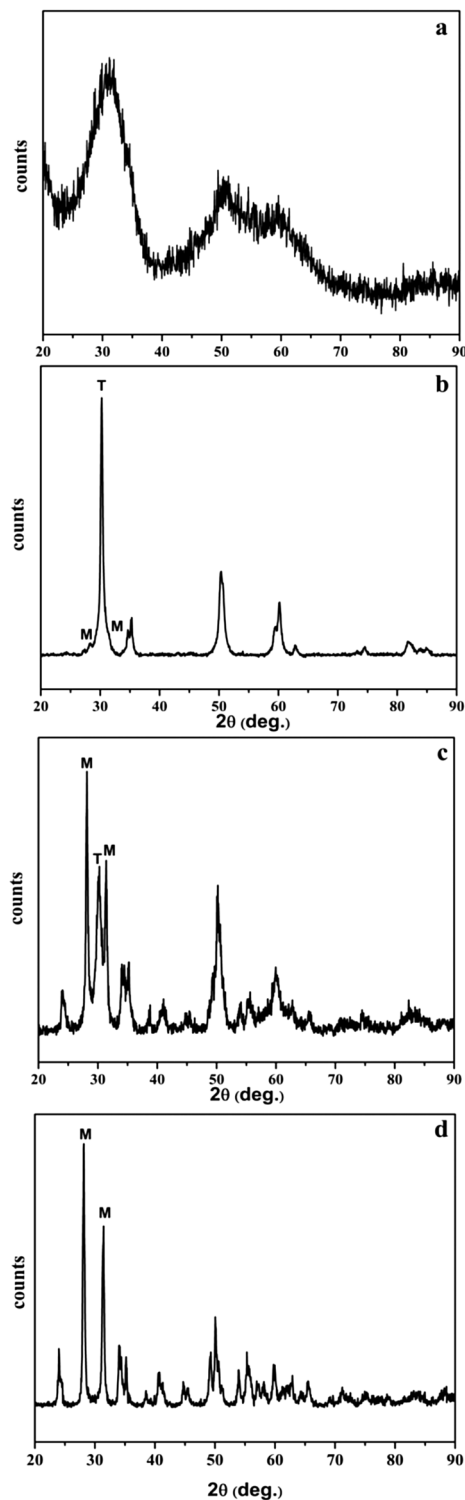


**Fig. 1** XRD pattern for zirconia nanoparticles (a) before annealing, (b) after annealing at 400 °C and (c) 600 °C, and (d) bulk zirconia. (T = tetragonal and M = monoclinic.)

results of this analysis are shown in the ESI.† The presence of each phase is identified by isolated peaks in the spectrum in the  $2\theta$  range of 25–35°. For example, the tetragonal phase has a large single peak at about  $2\theta = 30.1^\circ$ , but the monoclinic phase has two equal peaks located at  $2\theta = 28.20^\circ$  and  $31.49^\circ$ .<sup>28</sup> Both

annealed samples show the diffraction peaks associated with the monoclinic, tetragonal, and cubic phases. The limitations of using Rietveld refinements to discern nanoscale phases with similar spectra should be emphasized here. Tetragonal and cubic zirconia have very similar spectra, and the tetragonal phase can only be discerned reliably by the splitting of certain peaks, which are only visible in the absence of size-induced broadening. Therefore, it is plausible that  $\text{ZrO}_2$  spectra broadened by size effects would be more readily identified as tetragonal rather than cubic by a method such as Rietveld refinement.

Nonetheless, the cubic phase is not expected to form in the absence of dopant stabilizers and is the least stable in the temperature ranges we explored. The appearance of the cubic phase in the Rietveld refinement might be due to (i) the strong similarity in the position of the main peaks of the tetragonal and the cubic phase, combined with (ii) the fairly large spread in particle sizes (and therefore peak widths) observed in the sample ( $\sim 30\%$  polydispersity). Therefore, while we report the results of the Rietveld refinement as we obtained them, we believe that the fraction of cubic phase is probably to be attributed to the tetragonal phase.

As the samples are annealed at higher temperatures, two processes occur: the breadth of the XRD peaks decrease, and the atomic structure transitions towards the monoclinic phase. The reduced breadth of the peaks after annealing is expected due to the sintering of the particles and the consequent increase in the size of the crystallites and decrease in the surface area. An increase in the temperature of annealing leads to the emergence of the monoclinic phase, at the expense of the other phases (*cf.* Fig. 2), which is consistent with the expected role of annealing in bringing the structure closer to the phase that is more thermodynamically stable.

HR-TEM images of the as-synthesized nanoparticles and of the sample annealed at 400 °C show that the crystalline grains have an approximately spherical shape with an average size of 3.6 nm (Fig. 3a) and 6.1 nm (not shown), respectively. The size distribution of the grains (*cf.* Fig. 3b) was measured by TEM over 76 grains and yielded an approximately bell-shaped curve that could be adequately fitted with a Gaussian peak (center = 3.7 nm, width = 1.1 nm).

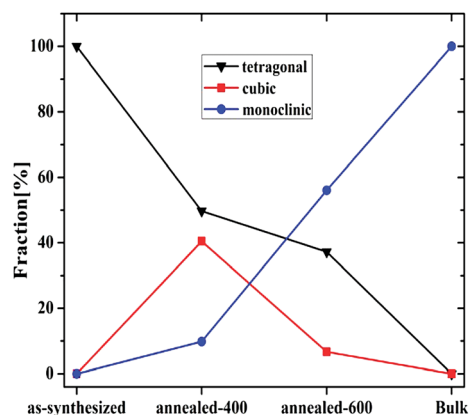


**Fig. 2** Phase composition of zirconia nanoparticles before and after annealing at different temperatures, and bulk zirconia.

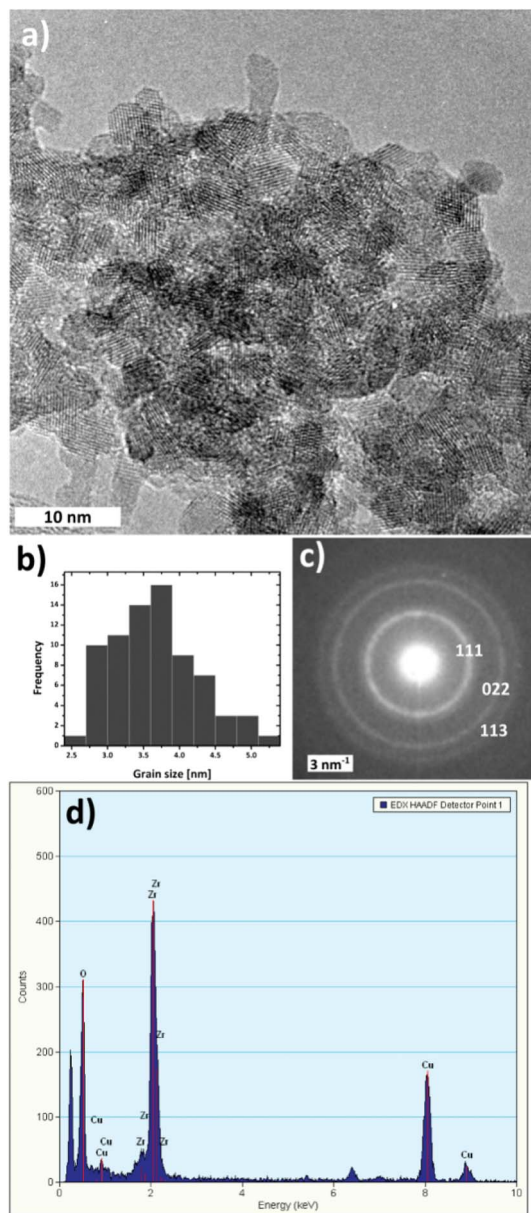


**Fig. 3** Electron microscopy characterization of as-synthesized  $\text{ZrO}_2$  nanoparticles. (a) HRTEM micrograph showing agglomerated particles. (b) Grain size distribution obtained from analysis of 75 grains. (c) SAED of particle agglomerates indicating the presence of crystallinity compatible with tetragonal structure. (d) EDAX spectrum of the sample; the Zr : O ratio is 1 : 2 within the experimental error of 3–4%.

The SAED (selected area electron diffraction) pattern obtained from the as-synthesized nanoparticles (*cf.* Fig. 3c) yielded diffraction features that could be indexed adequately with the tetragonal phase. It is also the case for SAED (as with XRD) that the similarity of the diffraction spectra does not allow us to determine unequivocally whether the phase is tetragonal or cubic. The stoichiometric ratio of Zr : O of the nanoparticles measured by EDAX (*cf.* Fig. 3d) was 1 : 2 within the experimental error of 3–4%. Within these limits of sensitivity, these EDAX data also suggest that the nanoparticles have no significant impurities: the signal from Cu and C was due to the carbon support film.

### 3.2 Catalytic activity study

The catalytic activity of the  $\text{ZrO}_2$  nanoparticles was assessed by using the Knoevenagel condensation of aldehydes and malononitrile. The reaction of benzaldehyde and malononitrile was selected as a model reaction and was optimized in different solvents. The best yield was obtained in ethanol (*cf.* Table 1). The effect of catalyst amount on the Knoevenagel condensation is shown in Table 2. The reaction yield in the absence of catalyst was negligible. Furthermore, different zirconia nanoparticle samples – as synthesized, annealed at 400 °C or at 600 °C – showed different activities (Table 3). The best yield (95% at 2 h) was obtained with the as-synthesized zirconia nanoparticles.

After we optimized the reaction conditions for a model reaction, we carried out Knoevenagel condensations in the presence of different aldehydes. Electron-deficient aldehydes gave the product more quickly than their electron-rich counterparts (*cf.* Table 4). To study the catalyst reusability, the catalyst recovered at the end of each reaction cycle was washed with methanol, dried, and reused for 3 consecutive cycles: the catalyst showed no loss in activity (*cf.* Table 5).

### 3.3 Effect of thermal treatment on the catalyst activity of $\text{ZrO}_2$ nanoparticles

Comparing the catalytic activity of  $\text{ZrO}_2$  nanoparticles with bulk powders is fraught with the difficulties associated with measuring quantitatively the activities of heterogeneous catalysts.<sup>29</sup> A number of parameters (some of which are hard or impossible to know precisely) can affect the activity: surface area, crystalline phase, structure of the exposed facets, nature of the active sites, interaction between active sites, surface reconstruction, effects of mass and heat transfer, *etc.* A detailed analysis of the activity of these particles is beyond the scope of this paper but we would like to report data that account for the obvious parameter: the surface area and crystalline phase of the catalysts. Textural properties of the zirconia nanoparticles are depicted in Table 6. The table shows that the unannealed sample has the largest surface area ( $\sim 60 \text{ m}^2 \text{ g}^{-1}$ ), followed by the sample annealed at 400 °C ( $\sim 48 \text{ m}^2 \text{ g}^{-1}$ ), at 600 °C ( $\sim 28 \text{ m}^2 \text{ g}^{-1}$ ) and bulk zirconia ( $\sim 10 \text{ m}^2 \text{ g}^{-1}$ ). The observed trend can be due to the annealing process, which results in the

**Table 1** Effect of solvent on the Knoevenagel reaction

Entry	Solvent	Time (h)	$T$ (°C)	Yield <sup>a,b</sup> (%)
1	Acetonitrile	3	82	41
2	<i>n</i> -Hexane	3	68	30
3	THF	3	66	68
4	Ethanol	2	78	95
5	Toluene	3	111	66
6	Dichloromethane	3	40	57
7	Methanol	2	65	73
8	Solvent-free	2	80	72
9	Water	3	100	25

<sup>a</sup> Yields of isolated products. <sup>b</sup> The reaction of benzaldehyde (1 mmol) and malononitrile (1.2 mmol) catalyzed by 0.02 g of unannealed  $\text{ZrO}_2$  in different solvents.

**Table 2** Influence of catalyst amount for the synthesis of 2-benzylidenemalononitrile. All reactions included 1 mmol of aldehyde, 1.2 mmol of malononitrile, and 5 mL of ethanol

Entry	Catalyst (g)	Time (h)	Yield <sup>a,b</sup> (%)
1	0.005	3	80
2	0.01	2	85
3	0.02	2	95
4	0.03	2	95
5	0.04	2	95

<sup>a</sup> Yields of isolated products. <sup>b</sup> The reaction of benzaldehyde (1 mmol) and malononitrile (1.2 mmol) catalyzed by 0.02 g of unannealed ZrO<sub>2</sub> in ethanol.

**Table 3** Phase-dependent catalytic performance of the zirconia nanoparticles for the synthesis of 2-benzylidenemalononitrile

Entry	Catalyst	Time (h)	Yield <sup>a,b</sup> (%)
1	Unannealed ZrO <sub>2</sub>	2	95
2	ZrO <sub>2</sub> -400	2	64
3	ZrO <sub>2</sub> -600	2	33
4	ZrO <sub>2</sub> bulk	4	10

<sup>a</sup> Yields of isolated products. <sup>b</sup> The reaction of benzaldehyde (1 mmol) and malononitrile (1.2 mmol) catalyzed by 0.02 g ZrO<sub>2</sub> in ethanol.

sintering and growth of nanoparticles leading to a decrease in the surface area.

**Table 5** Reusability of zirconia catalyst for the synthesis of 2-benzylidenemalononitrile<sup>a</sup>

Number of runs	Time (h)	Yield (%)
First	2	95
Second	2	95
Third	2	95

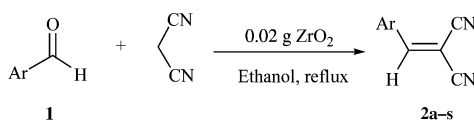
<sup>a</sup> The reaction of aldehyde (1 mmol) and malononitrile (1.2 mmol) catalyzed by 0.02 g ZrO<sub>2</sub> in ethanol.

**Table 6** Textural properties of zirconia nanoparticles

Sample	S <sub>BET</sub> <sup>a</sup>	D <sup>b</sup>
Unannealed ZrO <sub>2</sub>	60	3.5
ZrO <sub>2</sub> -400	48	3.9
ZrO <sub>2</sub> -600	28	5
ZrO <sub>2</sub> bulk	10	6.1

<sup>a</sup> Specific surface area (m<sup>2</sup> g<sup>-1</sup>). <sup>b</sup> Mean pore diameter (nm).

The variation in surface area is relatively modest when compared with the striking difference in catalytic activities. If we define the ratio of the yield to the surface area as an operational measure of activity, we obtain the histogram shown in Fig. 4. The unannealed sample shows a nearly 10-fold improvement in yield over the bulk sample, while the surface area is only 6 times higher.

**Table 4** Reaction of aldehydes with malononitrile<sup>a</sup>

Entry	Product	Ar	Time (h)	Yield <sup>b</sup> (%)	M.P. (°C)
1	2a	C <sub>6</sub> H <sub>5</sub>	2	95	84–85 (ref. 16)
2	2b	4-MeOC <sub>6</sub> H <sub>4</sub>	3	91	112–114 (ref. 17)
3	2c	4-MeC <sub>6</sub> H <sub>4</sub>	3	91	132–133 (ref. 16)
4	2d	3-MeC <sub>6</sub> H <sub>4</sub>	3	90	76–77
5	2e	2-MeC <sub>6</sub> H <sub>4</sub>	3	90	99–100
6	2f	2,4-(CH <sub>3</sub> O) <sub>2</sub> C <sub>6</sub> H <sub>3</sub>	3	91	143–145
7	2g	4-NO <sub>2</sub> C <sub>6</sub> H <sub>4</sub>	2	95	160–162 (ref. 18)
8	2h	3-NO <sub>2</sub> C <sub>6</sub> H <sub>4</sub>	2	94	101–102 (ref. 17)
9	2i	2-NO <sub>2</sub> C <sub>6</sub> H <sub>4</sub>	3	94	136–137 (ref. 19)
10	2j	4-ClC <sub>6</sub> H <sub>4</sub>	2	95	161–162 (ref. 20)
11	2k	3-ClC <sub>6</sub> H <sub>4</sub>	2	94	117–118
12	2l	2-ClC <sub>6</sub> H <sub>4</sub>	2	94	87–89 (ref. 21)
13	2m	2,6-Cl <sub>2</sub> C <sub>6</sub> H <sub>3</sub>	2	95	82–84
14	2n	4-BrC <sub>6</sub> H <sub>4</sub>	2	95	151–152 (ref. 19)
15	2o	2-Furyl	2	93	70–72 (ref. 22)
16	2p	2-Cinnamyl	2	91	124–126 (ref. 23)
17	2q	2-HO-C <sub>6</sub> H <sub>4</sub>	2.5	91	162 dec. (ref. 24)
18	2r	4-HO-C <sub>6</sub> H <sub>4</sub>	2.5	93	180–182 (ref. 23)
19	2s	4-Me <sub>2</sub> N-C <sub>6</sub> H <sub>4</sub>	2.5	93	179–180 (ref. 18)

<sup>a</sup> Yields of isolated products. <sup>b</sup> The reaction of aldehyde (1 mmol) and malononitrile (1.2 mmol) catalyzed by 0.02 g ZrO<sub>2</sub> in ethanol.

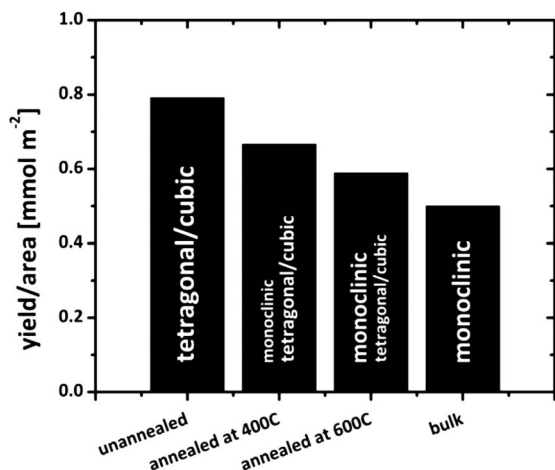


**Fig. 4** Estimation of catalyst activity as a function of thermal treatment (and the resulting difference in phase composition).

Even though a proper comparison of the catalytic activity of  $\text{ZrO}_2$  nanoparticles is inappropriate due to the differences in surface area, we cannot ignore the influence of crystalline phase in the catalyst activity. It is believed that the presence of oxygen vacancies, which are thought to be the most important factor for pure tetragonal zirconia stability as a consequence of the size effect, is responsible for the high activity of tetragonal zirconia.<sup>26</sup> Furthermore, most of the XRD studies on sulfated zirconia (SZ) catalysts show that the incorporated sulfate ions stabilize them in the metastable tetragonal phase.<sup>30</sup> In other words, the catalytic activity of SZ has been shown to be related to its crystal phase and specifically, tetragonal samples present higher catalyst activity than monoclinic samples.<sup>31</sup>

Studies by Vera *et al.* on the catalytic activity of sulfated zirconia showed that the existence of such oxygen vacancies provides active sites for catalyst activity.<sup>32</sup> According to a study by Reddy *et al.*,<sup>33</sup> unpromoted zirconia (*i.e.*, mainly consisting of monoclinic phase particles) exhibited negligible activity under identical reaction conditions compared with sulfated zirconia, which predominantly exists in the tetragonal phase.

In addition, Sasiambarrena *et al.* demonstrated the best catalytic performance was obtained from a sulfated zirconia (calcined at 550 °C) which showed tetragonal structure; lower activity was observed when the same catalyst was calcined at 800 °C and consisted of monoclinic phase particles.<sup>34</sup> We fully understand that this trend is to be considered as almost entirely qualitative, but it does point to a markedly increased activity of samples containing higher fractions of the non-monoclinic phases, even when the differences in surface area are taken into account. Our results are fully consistent with the hypothesis in which the nanoparticles are formed in a non-monoclinic structure (most likely tetragonal, or quasi-tetragonal) and they show a markedly high catalytic activity toward Knoevenagel condensation.

## 4. Conclusions

We have synthesized zirconia nanoparticles with a non-monoclinic structure. The synthesis was performed by thermally

decomposing zirconium oxychloride in the presence of oleylamine and oleic acid. The characterization of the material employed a variety of techniques and was complicated by the remarkably small size of the crystallites and the structural similarity of tetragonal and cubic zirconia. Nonetheless, the structural characterization and the high catalytic activity of the material towards the Knoevenagel condensation of aldehydes and malononitrile support the hypothesis that the as-synthesized material is in the tetragonal phase. This synthetic method has distinct practical advantages over previously reported approaches: (i) it avoids the use of dopants or high temperature annealing steps to stabilize the non-monoclinic phases, (ii) it uses less toxic and easily available reagents, (iii) it requires a relatively short reaction time, and (iv) it produces particulate material with remarkably small feature sizes ( $\sim 3$  nm) and a large expected surface area. The absence of injection steps (common in the synthesis of nanoparticles) suggests the possibility of developing this reaction further to a larger and more industrially-meaningful scale.

## Acknowledgements

RM thanks the University of Birjand for partial support of this work. The authors would like to express their sincere appreciation and gratitude to Dr Ludovico Cademartiri (Iowa State university) for his assistance and guidance in the preparation of this research paper.

## Notes and references

- 1 R. C. Garvie, R. H. Hannink and R. T. Pascoe, *Nature*, 1975, **258**, 703.
- 2 N. Mansour, K. Mansour, E. W. V. Stryland and M. J. Soileau, *J. Appl. Phys.*, 1990, **67**, 1475.
- 3 J. F. Haw, J. Zhang, K. Shimizu, T. N. Venkatraman, D. P. Luigi, W. Song, D. H. Barich and J. B. Nicholas, *J. Am. Chem. Soc.*, 2000, **122**, 12561.
- 4 S. P. S. Badwal, *Appl. Phys. A: Mater. Sci. Process.*, 1990, **50**, 449.
- 5 J. M. Phillips, *J. Appl. Phys.*, 1996, **79**, 1829.
- 6 C. Leon, M. L. Lucia and J. Santamaria, *Phys. Rev. B: Condens. Matter Mater. Phys.*, 1997, **55**, 882.
- 7 G. D. Wilk, R. M. Wallace and J. M. Anthony, *J. Appl. Phys.*, 2001, **89**, 5243.
- 8 (a) M. N. Tahir, L. Gorgishvili, J. Li, T. Gorelik, U. Kolb, L. Nasdala and W. Tremel, *Solid State Sci.*, 2007, **9**, 1105–1109; (b) G. Garnweitner, L. M. Goldenberg, O. V. Sakhno, Antonietti, M. Niederberger and J. Stumpe, *Small*, 2007, **3**, 1626; (c) F. Namavar, G. Wang, C. L. Cheung, R. F. Sabirianov, X. C. Zeng, W. N. Mei, J. Bai, J. R. Brewer, H. Haider and K. L. Garvin, *Nanotechnology*, 2007, **18**, 415702; (d) P. Shen and W. H. Lee, *Nano Lett.*, 2001, **1**, 707.
- 9 J. Kim, W. Myeong and S. Ihm, *Appl. Catal., B*, 2007, **71**, 57.
- 10 (a) M. Gateshki, V. Petkov, T. Hyeon, J. Joo, M. Niederberger and Y. Ren, *Solid State Commun.*, 2006, **138**, 279–284; (b) R. C. Garvie, *J. Phys. Chem.*, 1978, **82**, 218.

- 11 (a) J. Tang, J. Fabbri, R. D. Robinson, Y. Zhu, I. P. Herman, M. L. Steigerwald and L. E. Brus, *Chem. Mater.*, 2004, **16**, 1336; (b) R. C. Garvie, *J. Phys. Chem.*, 1965, **69**, 1238; (c) J. Joo, T. Yu, Y. W. Kim, H. M. Park, F. Wu, J. Z. Zhang and T. Hyeon, *J. Am. Chem. Soc.*, 2003, **125**, 6553.
- 12 M. Mizuno, Y. Sasaki, S. Lee and H. Katakura, *Langmuir*, 2006, **22**, 7137.
- 13 W. Li, H. Huang, H. Li, W. Zhang and H. Liu, *Langmuir*, 2008, **24**, 8358.
- 14 X. Xu and X. Wang, *Nano Res.*, 2009, **2**, 891.
- 15 L. Chen, T. Mashimo, E. Omurzak, H. Okudera, C. Iwamoto and A. Yoshiasa, *J. Phys. Chem. C*, 2011, **115**, 9370.
- 16 D.-Z. C. Xu, Y. Liu, S. Shi and Y. Wang, *Green Chem.*, 2010, **12**, 514.
- 17 Z. J. Ren and W. G. Cao, *Synth. Commun.*, 2002, **32**, 3475.
- 18 H. Moison, F. Texier-Boulet and A. Foucaud, *Tetrahedron*, 1987, **43**, 537.
- 19 L. Rong, X. Li, H. Wang, D. Shi, S. Tu and Q. Zhuang, *Synth. Commun.*, 2006, **36**, 2407.
- 20 S. Balalaie, M. Bararjanian, S. Hekmat and P. Salehi, *Synth. Commun.*, 2006, **36**, 2549.
- 21 X.-C. Yang, H. Jiang and W. Ye, *Synth. Commun.*, 2012, **42**, 309.
- 22 J. Zabicky, *J. Chem. Soc.*, 1961, 683.
- 23 C. Mukhopadhyay and A. Datta, *Synth. Commun.*, 2008, **38**, 2103.
- 24 J. A. Cabello, J. M. Campelo, A. Garcia, D. Luna and J. M. Matinas, *J. Org. Chem.*, 1984, **49**, 5195.
- 25 International Centre of Diffraction Data (ICCD), *Powder Diffraction File*, Newtown Square, PA, 2009.
- 26 (a) R. Grabowski, J. Sloczynski, M. Sliwa, D. Mucha, R. P. Socha, M. Lachowska and J. Skrzypek, *ACS Catal.*, 2011, **1**, 266; (b) W.-P. Dow, Y.-P. Wang and T.-J. Huang, *J. Catal.*, 1996, **160**, 155; (c) R. Li, I.-W. Chen and J. E. Penner-Hann, *J. Am. Ceram. Soc.*, 1994, **77**, 118; (d) H. Liu, L. Feng, X. Zhang and Q. Xue, *J. Phys. Chem.*, 1995, **99**, 332; (e) G. E. Rush, A. V. Chadwick, I. Kosacki and H. U. Anderson, *J. Phys. Chem. B*, 2000, **104**, 9597; (f) E. Karapetrova, R. Platzer, J. A. Gardner, E. Torne, J. A. Sommers and W. E. Evenson, *J. Am. Ceram. Soc.*, 2001, **84**, 65.
- 27 L. Cademartiri and V. Kitaev, *Nanoscale*, 2011, **3**, 3435.
- 28 J. Becker, P. Hald, M. Bremholm, J. S. Pedersen, J. Chevallier, S. B. Iversen and B. B. Iversen, *ACS Nano*, 2008, **2**, 1058.
- 29 M. Boudart, *Chem. Rev.*, 1995, **95**, 661.
- 30 (a) B. M. Reddy, M. K. Patil and B. T. Reddy, *Catal. Lett.*, 2008, **126**, 413; (b) B. M. Reddy and A. Khan, *Catal. Rev.*, 2005, **47**, 257.
- 31 (a) M. Hino, S. Kobayashi and K. Arata, *J. Am. Chem. Soc.*, 1979, **101**, 6439; (b) M. Hino and K. Arata, *J. Chem. Soc., Chem. Commun.*, 1980, 851; (c) C. Morterra, G. Cerrato, F. Pinna and M. Signoretto, *J. Catal.*, 1995, **157**, 109.
- 32 (a) C. R. Vera, J. C. Yori and J. M. Parera, *Appl. Catal., A*, 1998, **167**, 75; (b) C. R. Vera, C. L. Pieck, K. Shimizu and J. M. Parera, *Appl. Catal., A*, 2002, **230**, 137.
- 33 B. M. Reddy, M. K. Patil, K. N. Rao and G. K. J. Reddy, *J. Mol. Catal. A: Chem.*, 2006, **258**, 302.
- 34 L. D. Sasiambarrena, L. J. Mendez, M. A. Ocsachoque, A. S. Cánepa, R. D. Bravo and M. G. González, *Catal. Lett.*, 2010, **138**, 180.